NANO LETTERS

pubs.acs.org/NanoLett

Epitaxial Graphene on Cu(111)

Li Gao, Jeffrey R. Guest, and Nathan P. Guisinger*

Center for Nanoscale Materials, Argonne National Laboratory, Argonne, Illinois 60439

ABSTRACT The growth of graphene on single crystal Cu(111) has been achieved by thermal decomposition of ethylene in an ultrahigh vacuum chamber for the first time. The structural and electronic properties of graphene on Cu(111) have been investigated by scanning tunneling microscopy and spectroscopy. The nucleation of monolayer islands and two predominant domain orientations have been observed, which lead to the formation of numerous domain boundaries with increasing coverage. These results reveal that reducing the density of domain boundaries is one challenge of growing high-quality graphene on copper.

KEYWORDS Graphene, Cu(111), scanning tunneling microscopy

Graphene is nature's version of an ideal two-dimensional material that is comprised of a single sheet of hexagonally packed carbon atoms[1−3] and has long served as a building block for numerous carbon allotropes. Recently, the first electrical measurements made on isolated graphene have spurred a tremendous effort to explore the many unique properties of this material for a variety of applications.[4−10] The key challenges for utilizing graphene technology are controlling the graphene thickness and the ability to produce large area continuous sheets (of high quality with low defects). One promising approach has been the epitaxial growth of graphene on metal substrates by thermal decomposition of hydrocarbon or surface segregation of carbon atoms from the bulk metal.[11−17] Here we report the synthesis and characterization of graphene grown on single crystal Cu(111). Our growth was performed in an ultrahigh vacuum chamber (UHV), with both structural and electronic characterization carried out at the atomic-scale via scanning tunneling microscopy (STM). In addition to unique growth constraints on the single crystal, we have found that synthesis on Cu(111) involves the nucleation of monolayer islands of graphene that patch together like a quilt to form larger single-layer sheets, as a result there are numerous domain boundaries that scatter electrons and can affect carrier mobility. The overall interaction between the graphene and Cu(111) substrate results in the observation of two predominant Moiré patterns.

In chemical vapor deposition (CVD) growth studies on transition metals where carbon is soluble, the graphene forms when the sample is cooled and carbon segregates to the surface. The source of carbon is a result of the dissociation of organic precursor molecules on the substrate.[11] This growth mode can result in multiple grains of graphene with different thicknesses. Recently, large-area graphene sheets have been grown on Cu foil with relative ease via the decomposition of methane (CH_4) at high temperatures.[18] Unlike other transition metal substrates, in which graphene synthesis has been explored, carbon's solubility into Cu is extremely low.[19] Therefore, instead of surface segregation, the growth mode on Cu is quite different and mainly involves surface diffusion and nucleation of carbon atoms. In addition to the economic practicality of graphene synthesis on Cu, the low carbon solubility and growth kinetics limit the graphene thickness to predominantly a monolayer. This self-limiting growth and ability to transfer the resulting graphene films from the Cu foil propel this material system to the forefront for addressing the key challenges that face graphene technology.

The electron mobility in graphene is much higher than more traditional semiconductor materials, such as silicon. This high mobility makes graphene very attractive for electronic applications, but the mobility is also a good parameter to define the quality of the graphene films. The mobilities that were measured for graphene grown on Cu foil and subsequently transferred to SiO_2 are lower than those measured for graphene grown on SiC(0001) or mechanically exfoliated.[2,3,18] One argument for the lower mobility involves degradation of the graphene films as a result of the exposure to chemical processing that is used to remove the Cu foil substrate when transferring. However, one can also argue that the other forms of graphene with higher measured mobilities are also subjected to various chemical processing when patterning the device structure. The large area synthesis of graphene on Cu foil holds so much promise that it is important to determine the quality of the graphene as grown, which will help guide future optimization of the synthesis, transfer, and postprocessing. Therefore, we have studied the vacuum chamber growth of graphene on single crystal Cu(111) with UHV STM in order to provide well-characterized growth conditions as well as a platform for atomic-scale characterization.

The synthesis of graphene on single crystal Cu(111) (Figure 1a) was achieved by dissociating ethylene (C_2H_4) with

* To whom correspondence should be addressed, nguisinger@anl.gov. Corresponding author's address: Argonne National Laboratory, Center for Nanoscale Materials, 9700 South Cass Avenue, Bldg. 440, Argonne, IL 60439.
Received for review: 05/11/2010
Published on Web: 08/02/2010

DOI: 10.1021/nl1016706 | *Nano Lett.* **2010,** *10,* 3512–3516

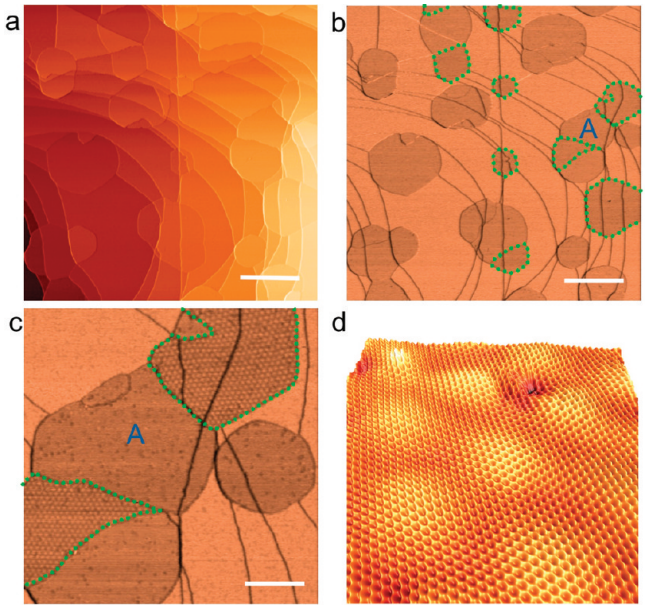

FIGURE 1. STM topography and differential conductance d*I*/d*V* images of graphene islands on Cu(111). (a) STM topography image of 0.35 monolayer of graphene on Cu(111). Scale bar: 200 nm. (b) Differential conductance d*I*/d*V* image ($U = -200$ mV) recorded simultaneously with the topography image (a). d*I*/d*V* signal can differentiate graphene from copper surface. Graphene shows dark contrast on this image. The areas highlighted with dotted lines are graphene domains showing Moiré patterns. Scale bar: 200 nm. (c) A close-up d*I*/d*V* image of a graphene island (marked with "A" in (b)). Scale bar: 60 nm. (d) Atomic resolution STM topography image of graphene showing the Moiré pattern and the honeycomb structure.

a pressure of 10^{-5} mbar at temperatures of ~1000 °C, very close to the melting point of Cu (1083 °C). The ethylene molecules were introduced into the UHV chamber through a leak valve and a nozzle which is about 2 cm from the Cu(111) surface. The pressure value was from the ion gauge for the preparation chamber. The actual ethylene pressure at the Cu(111) surface during growth is expected to be much higher than the readings of the ion gauge. Our first attempts to grow graphene involved exposing the crystal to ethylene for long periods of time at the growth temperature; this approach surprisingly resulted in almost no observable growth of graphene. This was not only counterintuitive but contrary to other CVD growth studies of graphene on different metals.[11] In order for us to successfully grow the graphene on single crystal Cu(111), repeated thermal cycling in a constant background of ethylene was necessary. This involved cooling to room temperature followed by a quick high-temperature (1000 °C) flash. We suspect that only the ethylene that adsorbs to the crystal at lower temperature contributes to dissociation and growth, while at high temperature the sticking probability of the ethylene becomes too low to contribute for our given background pressure. If this is correct, our graphene synthesis resembles more of an atomic layer deposition rather than traditional CVD growth. In our experiments, the coverage of graphene can be controlled by the number of thermal cycles. Four thermal cycles resulted in 0.35 monolayer of graphene, and eight thermal cycles resulted in 0.8 monolayer of graphene.

The graphene platelets are clearly resolved through scanning tunneling spectroscopy (STS) (Figure 1b, same area as the topography of Figure 1a); the contrast between the graphene and the Cu(111) within the 2D conductance map indicates a difference in the electronic structure at this particular energy. For this coverage, some of the graphene platelets are observed to extend continuously over the atomic step edges of the underlying substrate, while the majority have edges that terminate at Cu(111) step edges and appear to influence their shape. The resulting growth suggests a strong interaction between the surface diffusion of the graphene platelets and the migration of Cu(111) step edges at elevated temperatures. In areas with larger Cu(111) terraces (not shown), isolated graphene islands are observed. All of the observed graphene platelets and films are of single-layer thickness at both lower and higher graphene coverage.

For these tunneling conditions, there are regions of graphene in which a Moiré pattern is observed within the d*I*/d*V* conductance maps (outlined with green dashed lines in Figure 1b,c). The Moiré pattern is a result of overlaying the hexagonal lattice of the graphene with the hexagonal lattice of the Cu(111).[20] The nonhighlighted regions of graphene do in fact have a smaller Moiré pattern that is not observed at these tunneling conditions. It is clear, especially at higher resolution (Figure 1c), that there are different domains within the larger platelets of graphene. The nucleation and growth of individual platelets, which are mobile at elevated temperature, have edges that will stitch together with other platelets to form larger sheets resulting in different domains and domain boundaries. This is not initially apparent in the topographic data but is clearly observed utilizing STS. Atomic-resolution imaging of the graphene (Figure 1d) is easily achieved at higher tunneling currents.

It was difficult to observe both the smaller and larger Moiré patterns within a single image (Figure 2a), as a result of tunneling conditions and tip stability. The observation of multiple Moiré patterns, which is a result of different rotational alignments of the graphene lattice (2.46 Å) with the underlying Cu(111) lattice (2.56 Å), may indicate that the graphene is weakly coupled to the substrate. However, there are two predominant Moiré patterns that are observed, which suggests that the graphene does have preferred orientations with the underlying Cu(111). Any preferred orientation resulting from the interaction between the graphene and the substrate can influence the domain boundaries between platelets. An atomic-resolution image of the domain boundaries (Figure 2b) reveals a significant amount of electron scattering. There appears to be a periodic variation in height intensity and electron scattering patterns along the domain boundary, which is visible in both Figure 2a,b and resembles stitched fabric.

DOI: 10.1021/nl1016706 | *Nano Lett.* **2010,** *10,* 3512–3516

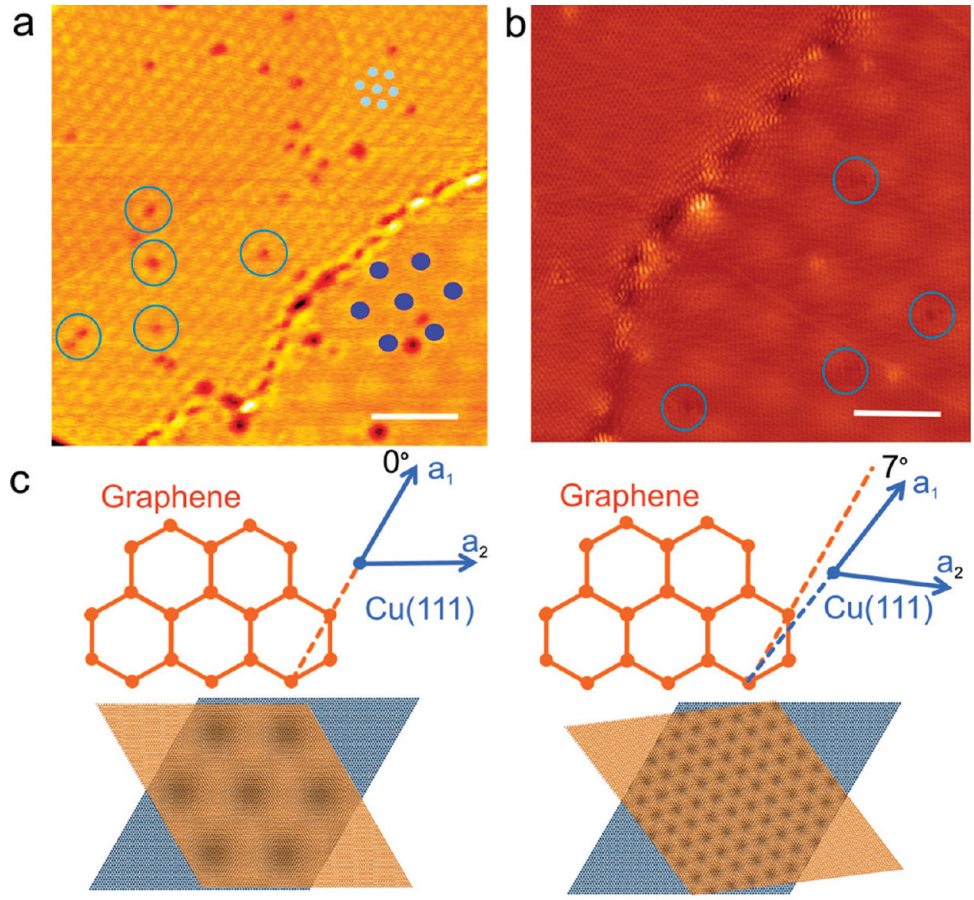

FIGURE 2. STM topography images at the domain boundaries of graphene on Cu(111) and two most observed Moiré patterns. (a) STM image at a domain boundary showing two different Moiré patterns in the two domains. The periodicity of the Moiré pattern for the upper left domain is ~2.0 nm, and that for the lower right domain is around 5.8 nm. Scale bar: 10 nm. (b) Atomic resolution STM image at a domain boundary, showing the honeycomb structure of graphene. The Moiré pattern in the upper left domain cannot be observed under this scanning condition. The periodicity of the Moiré pattern in the lower right domain is ~3.0 nm. Scale bar: 4 nm. Some adsorbates on the graphene surface are highlighted with blue circles in (a) and (b). (a) and (b) were recorded on different areas. (c) The most observed (~30%) Moiré pattern of graphene on Cu(111) with a periodicity of around 6.6 nm. The lattice orientation of graphene is strictly aligned with that of Cu(111). (d) Another typical Moiré pattern of graphene on Cu(111) with a periodicity of ~2.0 nm observed in our experiments. The misorientation angle is ~7°.

There are also several dark features speckled across the graphene and Cu(111) surface, some of which are highlighted with blue circles in Figure 2a,b. The dark features are in fact adsorbates, rather than defects in the graphene, that have frozen out during our imaging at 50 K. This is supported by the observation that all of the adsorbates (dark speckles) appear in the minimum of the Moiré pattern, where the influence of the local electronic structure on preferential adsorption is well-known.[20−23] The larger predominant Moiré pattern (~6.6 nm periodicity) can be reproduced when the graphene lattice is aligned with the Cu(111) lattice with a 0° rotation (Figure 2c). The smaller predominant Moiré pattern (~2 nm periodicity) is observed when we rotate our artificial graphene lattice by 7° with respect to the Cu(111).

In order to extract the electronic structure of the graphene with respect to the underlying Cu(111) substrate, a high density line of dI/dV spectra were measured over the region in Figure 3a. The two-dimensional conductance map of Figure 3b is the same area and has a green dashed line overlaid to spatially highlight our high density line of spectra. Individual spectra from this measurement are plotted in Figure 3c, where the red curve was measured over the graphene region and the green curve over the Cu(111). The peak for Cu(111)'s surface state is clearly visible at approximately −0.4 eV. At this energy we see the largest variation between the Cu(111) spectrum and the graphene. In the graphene spectrum the surface state of the underlying Cu(111) is clearly suppressed. There is also a dip in the spectrum at approximately −0.35 eV. This dip is reminiscent of a shift in the Dirac point that has been observed for graphene grown on SiC(0001). The electronic properties of graphene can be strongly influenced by interactions with the substrate. Without a secondary experimental technique, such as angle-resolved photoemission spectroscopy, it is difficult to assert that the dip is associated with the Dirac point. However, the dip is characteristic of all graphene regions and can be clearly seen as a blue band at −0.35 eV in the two-dimensional plotting of the spectrum (Figure 3d). It is also worth noting that the

DOI: 10.1021/nl1016706 | *Nano Lett.* **2010,** *10,* 3512–3516

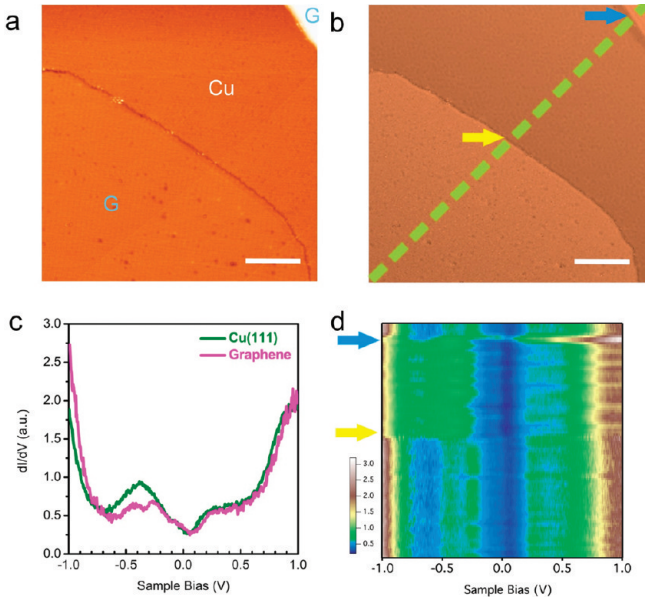

FIGURE 3. Scanning tunneling spectroscopy of graphene on Cu(111). (a) STM topography image showing both graphene (marked with "G") and Cu(111) (marked with "Cu"). Scale bar: 20 nm. (b) Differential conductance dI/dV image recorded simultaneously with the topography image (a). Graphene shows bright contrast. (c) dI/dV point spectra recorded on graphene and Cu(111). (d) dI/dV line map recorded at 100 points at equal distance along the dotted line in (b). The dI/dV spectra indicated by the arrows in (d) were recorded at the two boundaries between the graphene sheet and the Cu(111) substrate indicated by the arrows of the same colors in (b).

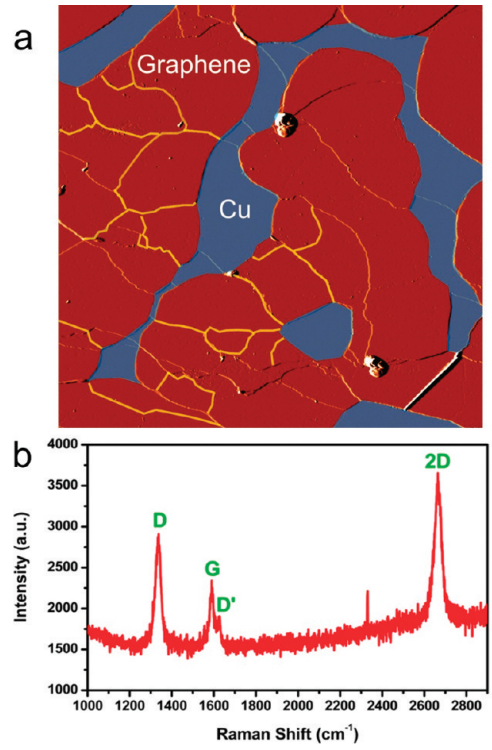

FIGURE 4. STM topography image and Raman spectroscopy of 0.8 monolayer of graphene on Cu(111). (a) STM topography image of 0.8 monolayer of graphene on Cu(111). The areas in blue are bare Cu(111) surface. Some domain boundaries of graphene are highlighted with yellow lines. Scan size: 500 × 500 nm^2. (b) Raman spectroscopy of 0.8 monolayer of graphene on Cu(111).

transition between the electronic structure of the graphene and Cu(111) regions (yellow arrow, Figure 3d) is very abrupt. The only variation at the transition from graphene to Cu(111) (blue arrow, Figure 3d) was a result of an atomic step edge of the substrate.

In addition to characterizing the initial stages of growth and electronic structure, we investigated higher graphene coverage (approaching a monolayer), as is illustrated in the STM topographic image of Figure 4a. In this image, regions of bare Cu have been highlighted blue, while the rest of the area is graphene. At the higher coverage graphene appears to form a continuous sheet across the surface. It is also evident that there are numerous domain boundaries that extend over the graphene sheet, some of which have been highlighted with yellow lines (Figure 4a). The presence of these domains, which we have shown to scatter electrons on the atomic scale (Figure 2b), can dramatically impact carrier transport and most likely play a role in the reduced carrier mobilities that have been reported for graphene grown on Cu foil.[18] In fact, it is hard to imagine that growth on polycrystalline foil would result in fewer domains. Raman spectra are measured on this sample at room temperature with a Raman microscope (Renishaw) at 633 nm excitation and show four primary features including a D band at ~1337 cm^{-1}, a G band at ~1590 cm^{-1}, a D′ band at ~1625 cm^{-1}, and a 2D band at ~2664 cm^{-1} (Figure 4b). The single layer thickness is verified by a ~0.5 G/2D intensity ratio and a symmetric 2D band with a full width at half-maximum of ~36 cm^{-1}.[24] The defect-induced bands D and D′ are most likely the result of exposed graphene edges and domain boundaries.[25,26] We are currently exploring ways to eliminate or heal these domain boundaries during synthesis.

In summary, we have successfully grown graphene on single crystal Cu(111) through the dissociation of ethylene at elevated temperatures. The single crystal growth in a vacuum chamber allows for ideal growth conditions and the atomic-scale characterization that is lacking in growth studies on polycrystalline Cu foil. Due to the low carbon solubility in Cu, we have found that carbon nucleates to form graphene platelets that chemically "stitch" together to form larger sheets. The result is numerous domain boundaries that clearly scatter electrons and will affect carrier mobility through the graphene sheet. These findings may explain the lower mobilities reported for graphene grown on Cu foil.

Acknowledgment. The use of the Center for Nanoscale Materials at Argonne National Laboratory was supported by the U.S. Department of Energy, Office of Science, Office of Basic Energy Sciences, under Contract No. DE-AC02-06CH11357. This work was also supported by the U.S. Department of Energy, "SISGR", Contract No. DE-FG02-09ER16109. The authors thank B. L. Fisher for his technical assistance.

DOI: 10.1021/nl1016706 | *Nano Lett.* **2010,** *10,* 3512–3516

REFERENCES AND NOTES

(1) Geim, A. K.; Novoselov, K. S. *Nat. Mater.* **2007**, *6*, 183–191.
(2) Fuhrer, M. S.; Lau, C. N.; MacDonald, A. H. *MRS Bull.* **2010**, *35*, 289–295.
(3) First, P. N.; de Heer, W. A.; Seyller, T.; Berger, C.; Stroscio, J. A.; Moon, J.-S. *MRS Bull.* **2010**, *35*, 296–305.
(4) Novoselov, K. S.; Geim, A. K.; Morozov, S. V.; Jiang, D.; Zhang, Y.; Dubonos, S. V.; Grigorieva, I. V.; Firsov, A. A. *Science* **2004**, *306*, 666–669.
(5) Novoselov, K. S.; Jiang, D.; Schedin, F.; Booth, T. J.; Khotkevich, V. V.; Morozov, S. V.; Geim, A. K. *Proc. Natl. Acad. Sci. U.S.A.* **2005**, *102*, 10451–10453.
(6) Berger, C.; Song, Z. M.; Li, T. B.; Li, X. B.; Ogbazghi, A. Y.; Feng, R.; Dai, Z. T.; Marchenkov, A. N.; Conrad, E. H.; First, P. N.; de Heer, W. A. *J. Phys. Chem. B* **2004**, *108*, 19912–19916.
(7) Novoselov, K. S.; Geim, A. K.; Morozov, S. V.; Jiang, D.; Katsnelson, M. I.; Grigorieva, I. V.; Dubonos, S. V.; Firsov, A. A. *Nature* **2005**, *438*, 197–200.
(8) Zhang, Y. B.; Tan, Y.-W.; Stormer, H. L.; Kim, P. *Nature* **2005**, *438*, 201–204.
(9) Geim, A. K. *Science* **2009**, *324*, 1530–1534.
(10) Ohta, T.; Bostwick, A.; Seyller, T.; Horn, K.; Rotenberg, E. *Science* **2006**, *313*, 951–954.
(11) Wintterlin, J.; Bocquet, M.-L. *Surf. Sci.* **2009**, *603*, 1841–1852.
(12) Sutter, P.; Flege, J. I.; Sutter, E. *Nat. Mater.* **2008**, *7*, 406–411.
(13) Coraux, J.; N'Diaye, A. T.; Busse, C.; Michely, T. *Nano Lett.* **2008**, *8*, 565–570.
(14) Yu, Q. K.; Lian, J.; Siriponglert, S.; Li, H.; Chen, Y. P.; Pei, S.-S. *Appl. Phys. Lett.* **2008**, *93*, 113103.
(15) Vázquez de Parga, A. L.; Calleja, F.; Borca, B.; Passeggi, M. C. G., Jr.; Hinarejos, J. J.; Guinea, F.; Miranda, R. *Phys. Rev. Lett.* **2008**, *100*, No. 056807.
(16) Marchini, S.; Günther, S.; Wintterlin, J. *Phys. Rev. B* **2007**, *76*, No. 075429.
(17) Pan, Y.; Zhang, H. G.; Shi, D. X.; Sun, J. T.; Du, S. X.; Liu, F.; Gao, H.-J. *Adv. Mater.* **2009**, *21*, 2777–2780.
(18) Li, X. S.; Cai, W. W.; An, J. H.; Kim, S.; Nah, J.; Yang, D. X.; Piner, R.; Velamakanni, A.; Jung, I.; Tutuc, E.; Banerjee, S. K.; Colombo, L.; Ruoff, R. S. *Science* **2009**, *324*, 1312–1314.
(19) Mclellan, R. B. *Scr. Metall.* **1969**, *3*, 389–391.
(20) N'Diaye, A. T.; Coraux, J.; Plasa, T. N.; Busse, C.; Michely, T. *New J. Phys.* **2008**, *10*, No. 043033.
(21) Sicot, M.; Bouvron, S.; Zander, O.; Rüdiger, U.; Dedkov, Y. S.; Fonin, M. *Appl. Phys. Lett.* **2010**, *96*, No. 093115.
(22) Donner, K.; Jakob, P. *J. Chem. Phys.* **2009**, *131*, 164701.
(23) N'Diaye, A. T.; Bleikamp, S.; Feibelman, P. J.; Michely, T. *Phys. Rev. Lett.* **2006**, *97*, 215501.
(24) Ferrari, A. C.; Meyer, J. C.; Scardaci, V.; Casiraghi, C.; Lazzeri, M.; Mauri, F.; Piscanec, S.; Jiang, D.; Novoselov, K. S.; Roth, S.; Geim, A. K. *Phys. Rev. Lett.* **2006**, *97*, 187401.
(25) Nemanich, R. J.; Solin, S. A. *Phys. Rev. B* **1979**, *20*, 392–401.
(26) Cancado, L. G.; Pimenta, M. A.; Neves, B. R. A.; Dantas, M. S. S.; Jorio, A. *Phys. Rev. Lett.* **2004**, *93*, 247401.

DOI: 10.1021/nl1016706 | *Nano Lett.* **2010,** *10,* 3512–-3516